On the Steady-State Energy Balance of Short Gravity Wave Systems

WILLIAM J. PLANT

U.S. Naval Research Laboratory, Washington, DC 20375

(Manuscript received 13 February 1980, in final form 6 May 1980)

ABSTRACT

Steady-state energy balances of short gravity wave systems generated in a wave tank with and without airflow have been measured and compared with the predictions of perturbation theory. Wind-wave spectra were found to fit a JONSWAP form to a good approximation if a wind-dependent equilibrium range coefficient was used. Mechanically generated waves were produced which had frequency spectra similar to wind-generated wave spectra and which exhibited nonlinear effects through a decrease in the spectral peak frequency with fetch. In the wind-wave case, perturbation theory well predicted the difference between the net source function and energy input from the wind for a wide range of fetch and wind speed conditions provided that surface tension was properly taken into account. In the case of waves generated without airflow, perturbation theory predicted energy transfer rates much smaller than the measured values.

1. Introduction

When a calm water surface is disturbed, waves are produced which eventually reach a state of dynamic equilibrium. Although energy transferred to the waves by the source of disturbance is finally removed from them by dissipative processes, the distribution of energy among various spectral components is largely determined by nonlinear properties of the waves. The most tractable approach to the treatment of water-wave nonlinearity is perturbation theory in which the wave system is considered to be comprised of weakly interacting Fourier components each of which satisfies a dispersion relation derivable from linear theory (Hasselmann, 1962, 1968; Valenzuela and Laing, 1972; Longuet-Higgins, 1976). Energy transfer between components occurs when resonance conditions on both frequency and wavenumber are met. Present theories impose the plausible and useful, but not essential, assumption that individual component waves are uncorrelated. Recently, this perturbation approach has been questioned by several authors who argue that nonlinear effects, especially in short gravity wave systems, negate not only the assumption of decorrelation but also the first-order dispersion relation (Lake and Yuen, 1978; Rikiishi, 1978; Toba, 1979).

Many experiments have been performed to test the assumptions and predictions of perturbation theory as applied to water waves. Plant and Wright (1979, 1980) demonstrated that dispersion relations of waves near the spectral peak of wind-wave systems in wave tanks may be derived from a linear theory if shear flow effects are taken into account. The 1969 JONSWAP experiments in the North Sea investigated nonlinear effects in the development of wind-generated gravity wave systems with fetch. Neither energy transferred from the wind nor lost through dissipation could be measured in this field study but the results generally confirmed the applicability of Hasselmann's third-order theory to energy balances in wave systems with dominant frequencies in the range of 0.2–0.5 Hz. Wu *et al.* (1977, 1979) measured energy fluxes due to nonlinear and dissipative processes for wind-generated waves in a wave tank when the wind speed was in the range of 7–9 m s^{-1} and peak spectral frequencies were from 2 to 5 Hz. They were able to fit their data with an approximation to Hasselmann's theory that was derived for a Pierson-Neumann spectrum (Barnett, 1966). They also attempted to determine the amount of dissipation due to wave breaking using a theory due to Hasselmann (1974) and found that near the spectral peak it was small compared to the energy transferred by nonlinear effects. Plant and Wright (1977) also measured energy fluxes for short gravity wave systems in a wave tank but arrived at a conclusion somewhat in opposition to that of Wu *et al.* They found that the second-order perturbation theory of Valenzuela and Laing (1972), which included the effects of surface tension, predicted energy fluxes adequate to explain the observations for dominant wave frequencies above 3.5 Hz.

In an effort to resolve questions about the adequacy of perturbation theory, with and without surface tension, for the description of energy fluxes

in short gravity wave systems, we have undertaken a detailed examination of the steady-state energy balance of wave systems with dominant wave frequencies between 1.65 and 6.5 Hz. Working in a wave tank, we have produced wind waves for a wide variety of wind speed and fetch conditions and have generated nonlinear wave systems in the absence of airflow using a loudspeaker system. We have attempted to fit our experimental results to a perturbation theory which is the sum of Hasselmann's (1962) theory and Valenzuela and Laing's (1972) theory. Technically, the effects of surface tension at third-order should be included in Hasselmann's theory for high dominant wave frequencies. As we shall see, however, second-order effects come to dominate at these frequencies so the theory has not been modified in our calculations. Thus we shall refer to Hasselmann's theory as the gravity wave theory and Valenzuela and Laing's theory as the gravity-capillary wave theory. Application of Longuet-Higgins' (1976) nonlinear theory for gravity waves to these data has not been attempted since maximum negative energy fluxes never occur at the dominant wave frequency. Note, however, that this theory yields energy fluxes of the same magnitude as that of Hasselmann (Fox, 1976). Recent work by Dungey and Hui (1979) indicates that maximum negative energy fluxes shift to higher frequencies for spectra of finite width, apparently reconciling Longuet-Higgins' work with that of Hasselmann.

Our results, detailed below, show that energy fluxes near the dominant wave frequency of wind-generated, short gravity wave systems may be explained by perturbation theory within experimental uncertainty for a wide range of wind speeds and fetches. If dissipation is also present in this frequency range, it must play a role subordinate to nonlinear processes at low and moderate wind speeds. For similar wave systems generated without airflow, however, current perturbation theory predicts less energy transfer than is observed.

2. Methods of investigation

Experiments were performed in an 18 m × 1.4 m wave tank which has a water depth of 30 cm and an air channel height of 30 cm. This tank has been described in detail in previous publications (Duncan *et al.*, 1974; Larson and Wright, 1975; Plant and Wright, 1977). Methods of generating wind waves and changing fetch and wind speed were identical in this study to those employed by Plant and Wright (1977). Relations between friction velocity and maximum wind speed as well as dominant wave frequency versus fetch are also given in that publication.

The loudspeaker system for generating waves without airflow has not been described previously

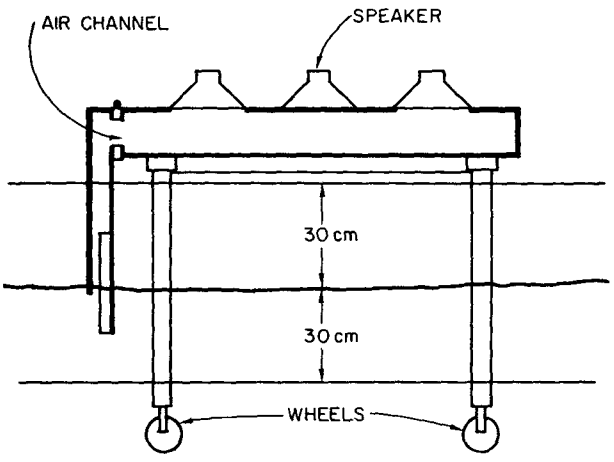

FIG. 1. Schematic diagram of loudspeaker system.

and is shown schematically in Fig. 1. The apparatus consists of five high-compliance woofers, each 15 inches in diameter, mounted on top of a hollow, airtight wooden chamber. The chamber rests above the wave tank on a rolling cart. One end of the chamber is connected to a hinged duct which, in its vertical position, contacts the water surface at the lower end. Thus an air channel is created between the speakers and the water surface so that a localized area of the surface may be elevated or depressed by the action of the speakers. The water surface upon which the speakers act is a strip of length equal to the tank width and of width which is variable from 1 to 5 cm.

The speakers were connected in series and driven, through a power amplifier, by an FM tape recorder. Our procedure was to generate wind waves in the tank with the hinged duct of the speaker system raised to allow passage of the wind. A capacitance-type wave gage (Plant and Wright, 1977) was mounted in the tank to monitor these waves. The output of this gage was recorded on tape, the wind turned off, the duct lowered and the tape played back through the loudspeaker system. In this manner, short gravity wave systems could be produced without airflow but having spectra similar to those of wind-generated waves. Details of the spectra produced by this system are given in Section 4.

Three methods, besides the capacitance probe mentioned above, were used to measure properties of wave systems. These were Cox's optical method for measuring wave slopes (Cox, 1958), microwave Doppler spectrometry (Plant and Wright, 1977) and the photographic technique of Stillwell (Stillwell, 1974; Keller and Pilon, 1980). We used Cox's method to obtain most wave-height spectra reported here because of its simplicity and ease of calibration, and because we felt that it gave a more reliable measurement than the capacitance probe at

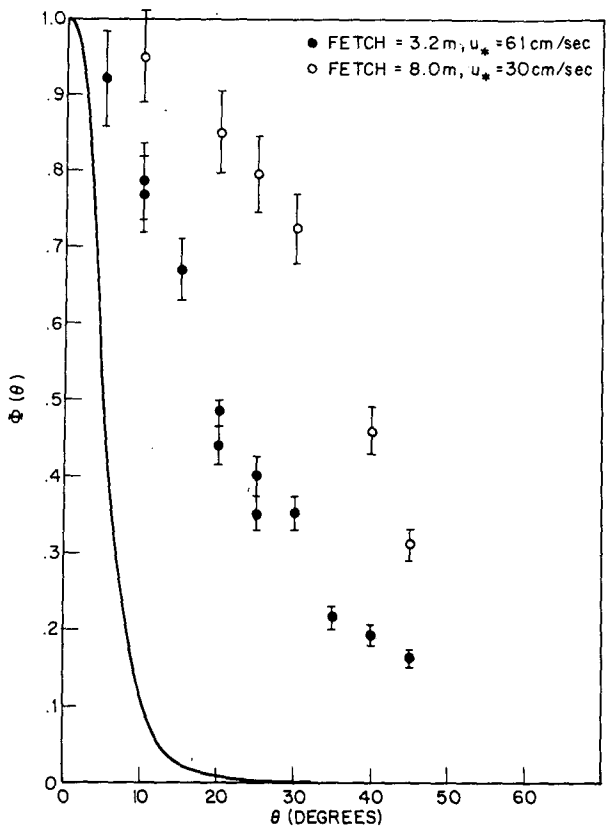

FIG. 2. Angular distribution of wind waves. $\Phi(\theta)$ is the ratio of the spectral intensity in the direction θ to that along the wind direction. The solid line indicates the angular dependence of the antenna pattern.

high frequencies. Microwave Doppler spectrometry provides a convenient method of investigating angular spreading functions of spectra while Stillwell's technique provides wavenumber spectra of capillary waves. Each of these techniques is described in detail in the indicated references, so we shall only briefly describe our implementation here.

Cox's method consists of focusing a telescope on the water surface and masking the ocular except for a small hole. Light passed by this hole originates from a small spot on the water surface; in our experiments, the spot diameter was 0.7 mm as determined by illuminating the surface through the telescope. A graded source of illumination is placed below the water surface with the gradient along the axis of the tank. With waves present on the surface, the intensity of light received by the telescope depends on the instantaneous, upwind-downwind slope of the waves. This illumination is sensed by a photomultiplier tube mounted above the telescope. The output of the photomultiplier deviated from proportionality to surface slope by less than 5% for slopes up to 40°. The system was calibrated frequently by simply moving the telescope along the tank axis.

In the technique of microwave Doppler spectrometry, coherent microwave radiation is backscattered from a roughened water surface. The backscattered power is proportional to the spectral density of the wave system at a wavenumber which is resonant with the microwave parameters. In particular, the system responds to a small region of water wavenumbers (k_x,k_y) in the neighborhood of $(2k_0 \cos\theta,0)$ where the x axis is the horizontal projection of the direction in which the antenna is pointed, k_0 the microwavenumber and θ the grazing angle. The backscattered signal is Doppler-shifted by an amount which is identically equal to the water-wave frequency.

In our primary implementation, the microwave system was operated at 1.85 GHz and illuminated an area which included that viewed by the telescope. Thus simultaneous microwave and optical measurements were possible. Depression angles of the microwave antennas were fixed at 60° during most experiments in order to allow the azimuth angle to be varied. This yielded a Bragg wavenumber of 0.41 cm^{-1} or a wavelength of 15.3 cm. In the few experiments which were run with variable depression angles, the azimuth angle was fixed along the tank axis. In these cases, simultaneous optical and microwave measurements were not possible.

The photographic technique as implemented in our wave tank consists of photographing the roughened water surface with a camera above the tank and pointed in the nadir direction. A synchronized burst of graded illumination is emitted below the tank when the shutter of the camera is opened. Again, the gradient of illumination is upwind-downwind and the light intensity varied linearly along the tank. Negatives of film exposed in this manner are placed on an optical bench and Fourier-transformed. Sampling various points in the transform plane using a photomultiplier then yields upwind-downwind slope spectra for various wavenumbers. The wavenumber range accessible with this technique was 2–15 cm^{-1}.

To compare results of experiments with gravity wave theory, the numerical techniques used by Valenzuela and Wright (1979) were employed. Briefly, a copy of a computer program developed by Hasselmann and Sell was modified to run on a Texas Instruments Advanced Scientific Computer for frequencies in the range of 1.5–7 Hz. Computations from the program after these modifications were compared with energy transfers calculated by Hasselmann and Sell using the original form of the program. The results, scaled according to formulas of Hasselmann *et al.* (1973), were always within 5% of the original calculations.

Energy flux due to the gravity-capillary interaction was obtained from formulas derived by Plant (1978) from the original equations of Valen-

zuela and Laing (1972). The derivation simplified the original theory by considering the special case where the wave of interest is a short gravity wave. Wind speed effects were included in an ad hoc manner by requiring the dispersion relation to conform to those measured in previous wave tank experiments, that is, by including advection due to the wind drift (Plant and Wright, 1980).

3. Wind-generated waves

Slope spectra of wind waves were obtained for a variety of wind speeds and fetches using Cox's technique. These spectra were produced by a Nicolet Scientific UA500 A Spectrum Analyzer using a resolution of 0.04 Hz and averaging 64 individual spectra. The slope probe was calibrated after every second run. It was found that this calibration changed rather rapidly for the first 2 h after the system was activated, with slower drifts occurring after this time. Thus a warm-up period was allowed each day before spectra were taken. Subsequent calibration drifts were fully taken into account in the spectral determination. While the slope probe was reaching equilibrium each day, the water surface was swept clean of contaminants using a high wind. We estimate the accuracy of our spectral values to be ±25%.

Conversion of these slope spectra to displacement spectra was readily achieved through the relation

$$S(f) = k^2 E(f) \int \psi(\theta) \cos^2\theta d\theta, \qquad (1)$$

where $S(f)$ and $E(f)$ are slope and displacement spectral densities, respectively, k is the wavenumber of the wave of frequency f, and an angular spreading factor $\psi(\theta)$ that is independent of frequency has been assumed. Here $\psi(\theta)$ is normalized so that $\int \psi(\theta)d\theta = 1$ and θ is measured from the tank axis looking upwind. We measured the dispersion relation (Plant and Wright, 1979, 1980) and the angular spreading factor using microwave Doppler spectroscopy. Fig. 2 shows the angular distribution of waves of wavenumber 0.41 cm^{-1} for fetches of 3.2 and 8.0 m in terms of $\Phi(\theta) = \psi(\theta)/\psi(0)$. To indicate the angular resolution of these measurements, the solid line gives the azimuthal pattern of the antenna measured using monochromatic surface waves as described by Plant and Wright (1977). Wind speed has been adjusted so that 0.41 cm^{-1} waves were dominant waves in both cases. If we assume that spectral energy is negligible for $|\theta| > \pi/2$, we find that the integral in Eq. (1) varies from about 0.75 for 8.0 m fetch to about 0.92 for 3.2 m fetch. In view of the uncertainty in the assumption that ψ is independent of f and in the experimental measurement of $S(f)$, we have ignored this small fetch dependence of the integral and have adopted a $\cos^2\theta$ angular dependence throughout the wind-wave study. Thus,

$$S(f) = \tfrac{3}{4}k^2 E(f). \qquad (2)$$

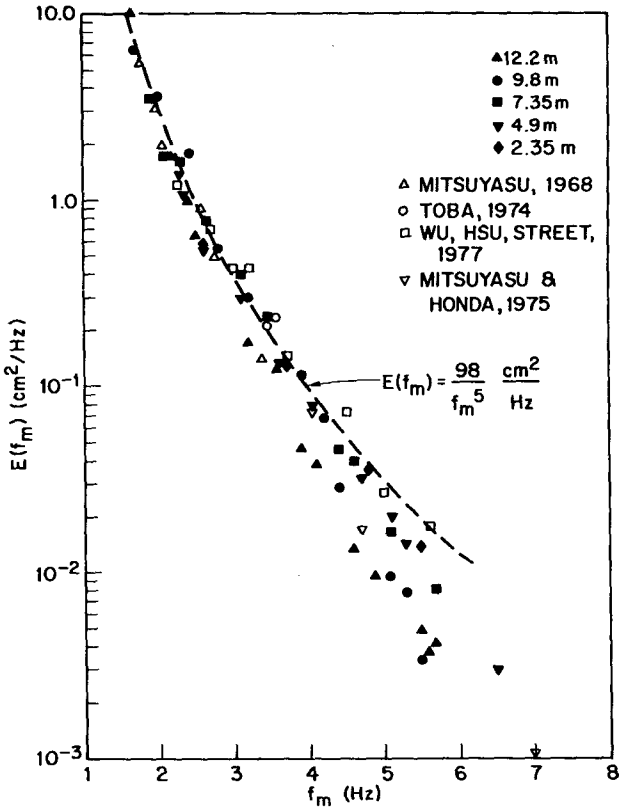

FIG. 3. Spectral density at the dominant wave frequency versus that frequency.

Spectral densities at the dominant wave frequency $E(f_m)$ determined from our experiments are shown in Fig. 3 as a function of f_m. Here we also plot values of $E(f_m)$ determined by other investigators (Mitsuyasu, 1968; Toba, 1974; Mitsuyasu and Honda, 1975; Wu *et al.*, 1977). The dashed line shows the value of $E(f_m)$ obtained by fitting data taken at high winds to a JONSWAP-type spectrum (Hasselmann *et al.*, 1973):

$$E(f) = \alpha g^2 (2\pi)^{-4} f^{-5} \exp\left[-\frac{5}{4}\left(\frac{f}{f_m}\right)^{-4}\right] \times \gamma^{\exp[-(1-f/f_m)^2/2\sigma^2]}. \qquad (3)$$

For a given f_m, our data are found to fit this curve at short fetches but fall below it as the fetch increases, i.e., as the wind speed drops. Thus $E(f)$ is more properly $E(f,x,u_*)$ but, for notational convenience, x and u_* will be suppressed.

Spectra measured in our tank exhibited a self-

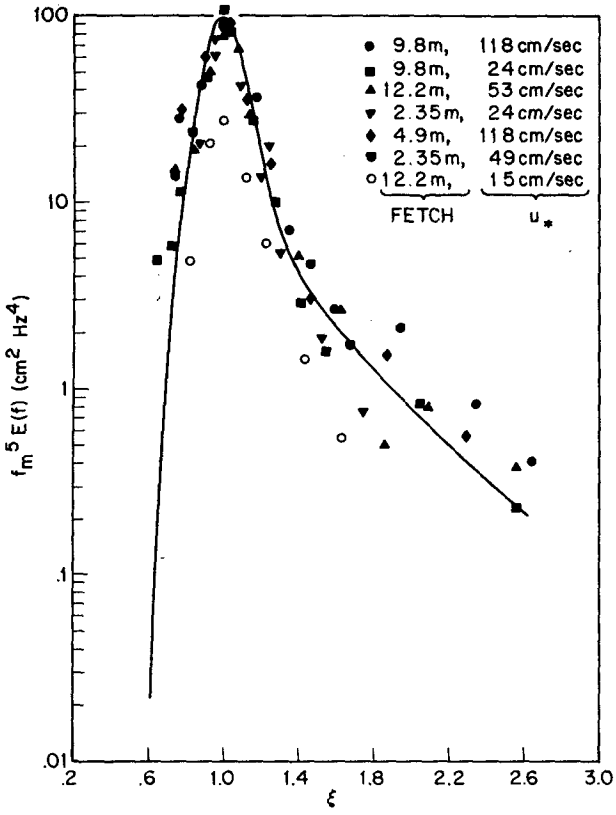

FIG. 4. Spectral data versus normalized frequency $\xi = f/f_m$. Curve shows a JONSWAP spectrum with $\alpha = 0.044$, $\gamma = 12.6$ and $\sigma = 0.16$.

similar form as shown in Fig. 4. Here we plot spectral densities multiplied by f_m^5 as a function of f/f_m which we shall call ξ. With the exception of the open circles, the data are fit well by the curve which shows $f_m^5 E(f)$ for a JONSWAP spectrum with

$$\alpha = 0.044, \quad \gamma = 12.6, \quad \sigma = 0.16. \tag{4}$$

The open circles in this figure represent data taken at very low winds. These data still retain the shape of a JONSWAP spectrum but with a decreased magnitude. We found that spectra in our tank could be fit to the JONSWAP form at all wind speeds by allowing α to vary with wind speed as shown in Fig. 5a.

The parameters given in Eq. (4) were obtained from data taken in our tank with $u_* > 80$ cm s^{-1}. The parameter α was obtained by fitting data in the range $1.6 f_m \leq f \leq 2.4 f_m$, γ was obtained from the spectral peak, and σ was determined by the width of the spectrum near the peak. For lower wind speeds, α was obtained by fitting $E(f_m)$. For self-similar spectra of the JONSWAP type, we may calculate the mean-square upwind/downwind dominant wave slope using Eq. (2) and (3):

$$\overline{S_D^2} = (3/4) \int_0^{1.6 f_m} k^2 \alpha g^2 (2\pi)^{-4} f_m^{-5} \psi'(\xi) df, \tag{5}$$

where $\psi'(\xi) = E(f)/[\alpha g^2 (2\pi)^{-4} f_m^{-5}]$, and integrating only to $1.6 f_m$ limits us to the dominant wave slope. If wind speed effects on the dispersion relation are neglected,

$$k^2 = (2\pi f)^4 / g^2, \tag{6}$$

$$\overline{S_D^2} = \tfrac{3}{4} \alpha \int_0^{1.6} \xi^4 \psi'(\xi) d\xi. \tag{7}$$

Since the integral has a value of about 1.1 for the spectrum of Fig. 4,

$$\overline{S_D^2} = 0.83\alpha. \tag{8}$$

Thus the saturation of α with increasing wind is to be expected since the dominant wave reaches a constant mean-square slope as shown in Fig. 5b. The saturation value of $\overline{S_D^2}$ given by Eqs. (4) and (8) is 0.036, which is slightly higher than that shown in Fig. 5b because of the neglect of the effects of wind speed in Eq. (6).

It is of interest to compare the spectral values measured here with those of other investigators. Parameters γ and σ given in Eq. (4) are approximately constant, as were the corresponding parameters determined in the JONSWAP experiments, although our values show that short gravity wave spectra are more peaked than their counterparts for systems of longer waves. Our parameter α, when plotted against nondimensional fetch $\hat{x} = xg/u_*$, falls along a line parallel to but lower than the JONSWAP curve for $\hat{x} > 5 \times 10^2$. For lower values of $\hat{x}$, our α saturates as it must because of its relationship to the dominant wave slope. The parameter α determined here is also generally smaller than those derived from the high-frequency tail of the spectrum in wave-tank experiments (Mitsuyasu, 1968; Mitsuyasu and Honda, 1975). There is probably a logical nonsequitor involved in comparing values derived by the two methods, however, since it is not obvious why the spectral density near the peak should be related to that in the tail. In any event, only measurements near spectral peaks concern us here.

These spectral measurements may be used to determine the sum of nonlinear energy transfer S_{nl} and dissipation S_d in the steady state using the energy balance equation (Hasselmann, 1968)

$$S_{nl} + S_d = c_g \frac{\partial E}{\partial x} - \beta E, \tag{9}$$

where β is the growth rate of waves due to wind and c_g is group velocity. In Eq. (9), we have taken the energy transferred from the wind to be proportional to spectral density in conformity with a variety of initial growth rate measurements (Hidy

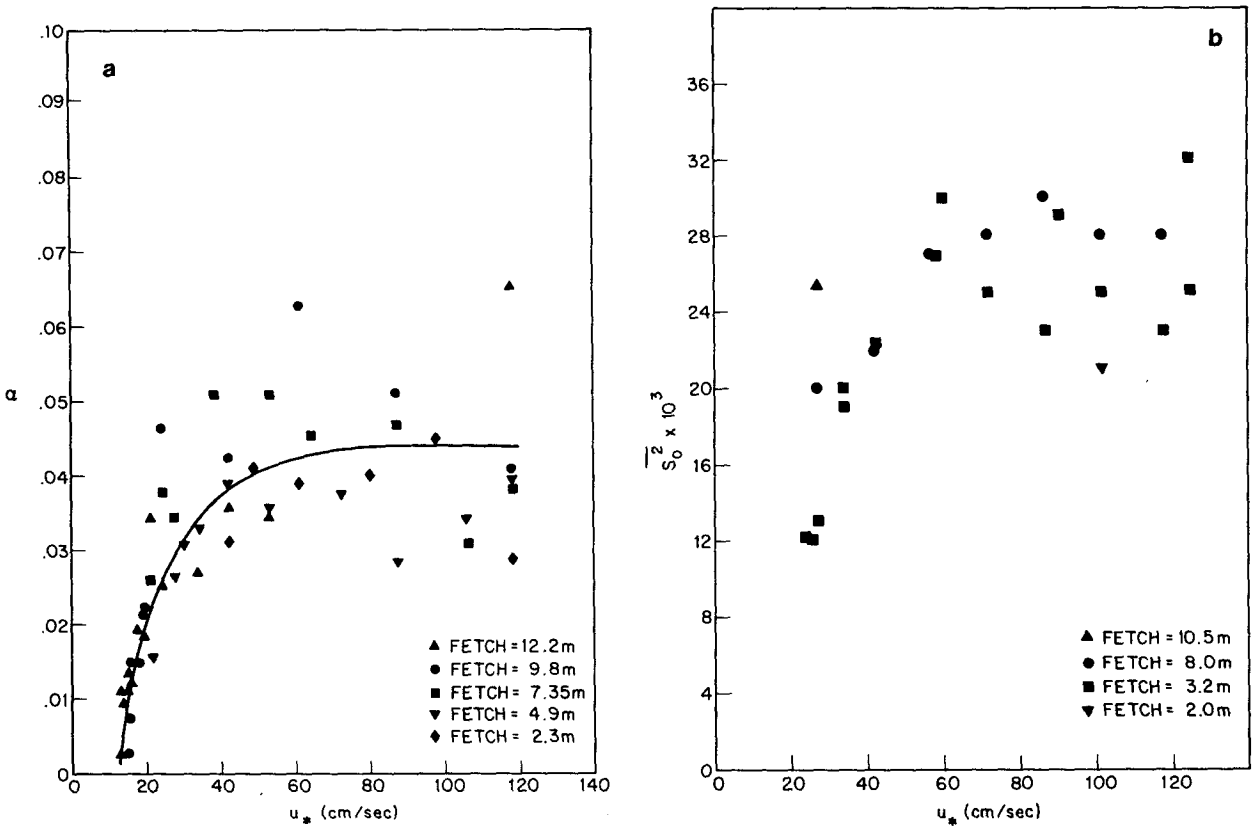

FIG. 5. (a) The parameter α versus friction velocity. Curve is empirical fit used in this study. (b) Upwind/downwind dominant wave slope versus friction velocity.

and Plate, 1966; Larson and Wright, 1975; Plant and Wright, 1977). The values of energy flux from the wind, S_{in}, which we shall actually use, however, also fit those of Wu *et al.* (1977, 1979) which were steady-state measurements.

Wu *et al.* correlated the pressure above wave crests with wave height to obtain S_{in} ($=\beta E$). Fig. 6 shows their values of S_{in} divided by $E(k)$ as a function of wavenumber. Also shown are β values determined from microwave measurements of initial growth rates. The figure shows that the microwave values at $k > 0.6$ cm^{-1} and Wu *et al.*'s values are fit rather well by curves given by

$$\beta = 0.04 u_*^2 k c^{-1} - 4\nu k^2 \tag{10}$$

when c has the wind-dependence observed by Plant and Wright (1980) and ν is the kinematic viscosity. This equation has been shown to imply that the stress supported by the waves, $\rho_w \int [\beta E(f)/c] df$, is approximately equal to the wind stress, $\rho_a u_*^2$ (Larson and Wright, 1975). Eq. (10) will be used to determine S_{in} in this study. The higher values of β measured during initial growth for $k < 0.6$ cm^{-1} have been interpreted as being due to nonlinear transfer in addition to direct input from the wind (Plant and Wright, 1977).

Values of $\partial E(f)/\partial x$ may be determined from measured spectra in two ways, either by measuring $E(f)$ as a function of fetch and obtaining the derivative from curves or by using Eq. (3) along with values of f_m for various fetches and windspeeds. For the latter method, we have

$$\frac{\partial E(f)}{\partial x} = \frac{\partial E(f)}{\partial f_m} \frac{\partial f_m}{\partial x} \tag{11}$$

since fetch dependence of spectral parameters other than f_m was not observed in our tank. Dominant wave frequencies in our tank are well fit by the empirical expression

$$f_m = \frac{96}{x^{1/3} u_*^{1/3}} \left(\frac{60}{u_*} \right)^{80/x}, \tag{12}$$

where cgs units are used. This expression reduces to the JONSWAP expression for large fetches. We may therefore compute

$$\frac{\partial E(f)}{\partial x} = \frac{E(f)}{x} \left\{ \frac{5}{\xi^5} + 99\xi(1 - \xi) \times \exp\left[-\frac{(1 - \xi)^2}{0.0512} \right] \right\} \left\{ \frac{1}{3} + \frac{80 \ln(60/u_*)}{x} \right\}. \tag{13}$$

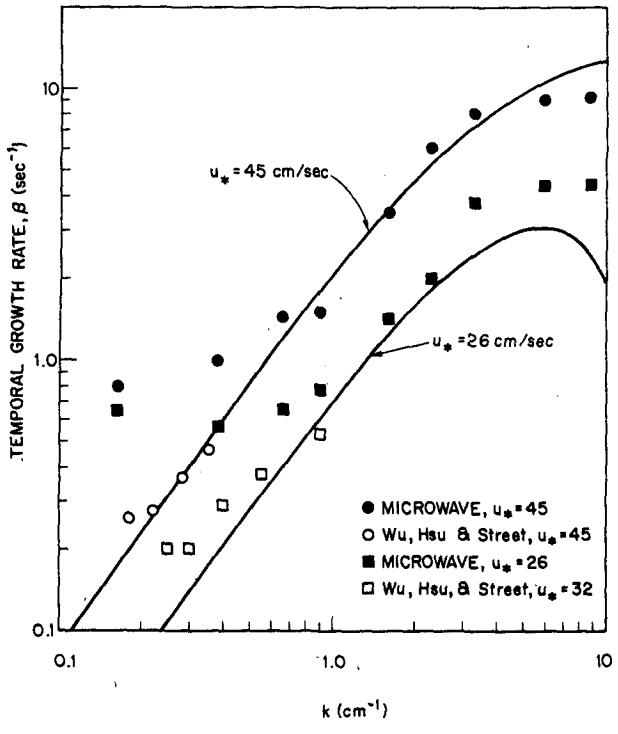

FIG. 6. Temporal growth rate $\beta = S_{in}/E$ versus wavenumber. Curves show $\beta = 0.04u_*^2k/c - 4\nu k^2$ with a wind-dependent c.

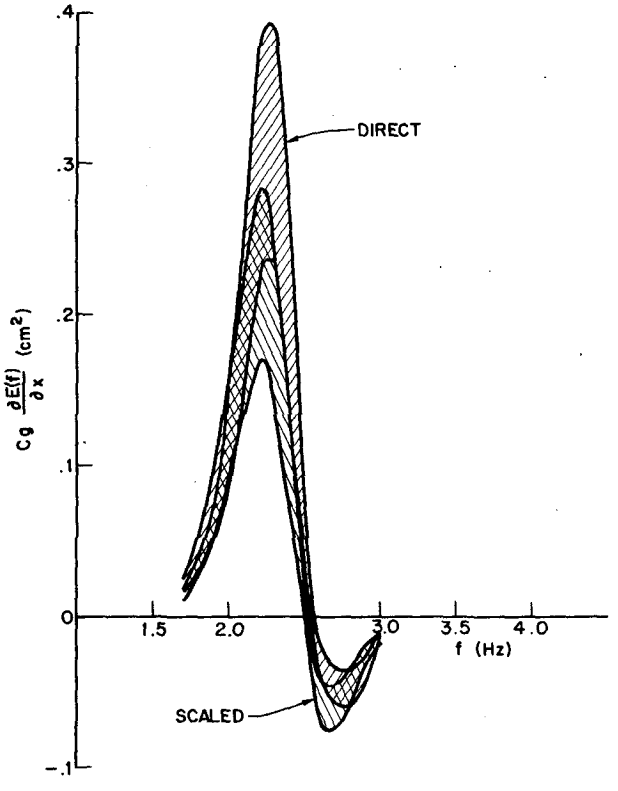

FIG. 7. Net source function determined directly from $E(f)$ versus fetch and from scaling formula.

Fig. 7 compares values of $c_g\partial E(f)/\partial x$ computed by this scaling method with those derived by the more direct method. Experimental uncertainties are indicated by the shaded areas. In both cases c_g has been obtained from dispersion curves derived from microwave scattering. Since the two methods yield comparable results and the computations are easier using Eq. (13), this method has been employed to determine the net source function $c_g\partial E(f)/\partial x$ in this study. Values of $c_g\partial E/\partial x$ and βE for three different dominant wave frequencies and $u_* = 15$ cm s^{-1} are shown in Fig. 8.

As previously indicated, we attempted to fit these experimental data using the gravity wave and gravity-capillary wave theories. The gravity wave theory scales according to

$$S_{nl}^{gg}(f) = \alpha^3 f_m^{-4}\Lambda(\xi) \qquad (14)$$

as given by Hasselmann *et al.* (1973). Here $\Lambda(\xi)$ is a function which depends on spectral shape and is shown in Fig. 9 for our self-similar, short gravity wave spectrum. From this function, values of $S_{nl}^{gg}(f)$ can be obtained for any fetch and wind speed in our wave tank.

The gravity-capillary wave interaction was found by Plant (1978) to be given to a good approximation by

$$S_{nl}^{gc}(f) = -[92.2(2\pi)Cfk/k_l]E(f) \qquad (15)$$

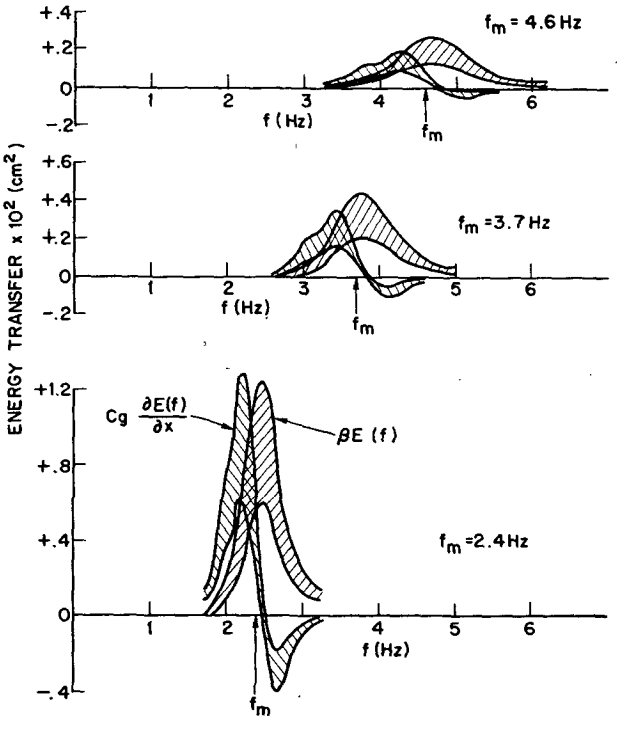

FIG. 8. Net source function and energy input from wind versus frequency for three different peak frequencies and $u_* = 15$ cm s^{-1}.

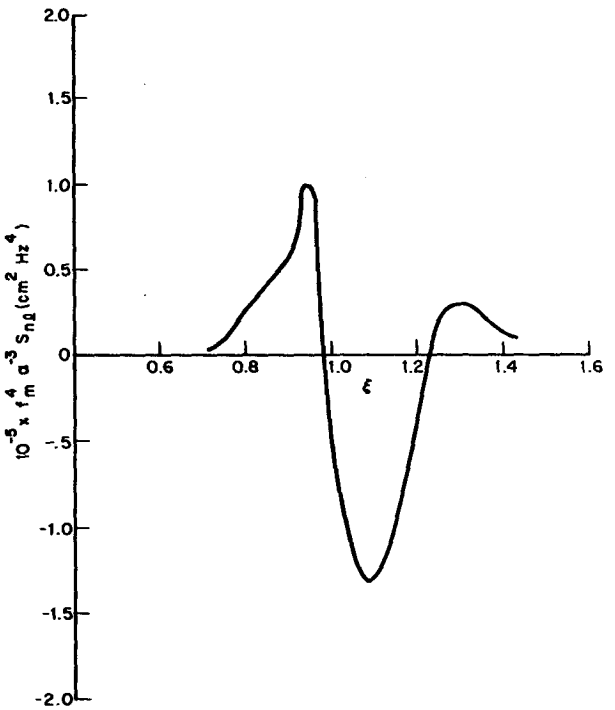

FIG. 9. Shape-dependent theoretical function $\Lambda(\xi)(=\alpha^{-3} f_m^{+4} S_{nl}^{gg})$ for wave tank spectra versus normalized frequency $\xi = f/f_m$.

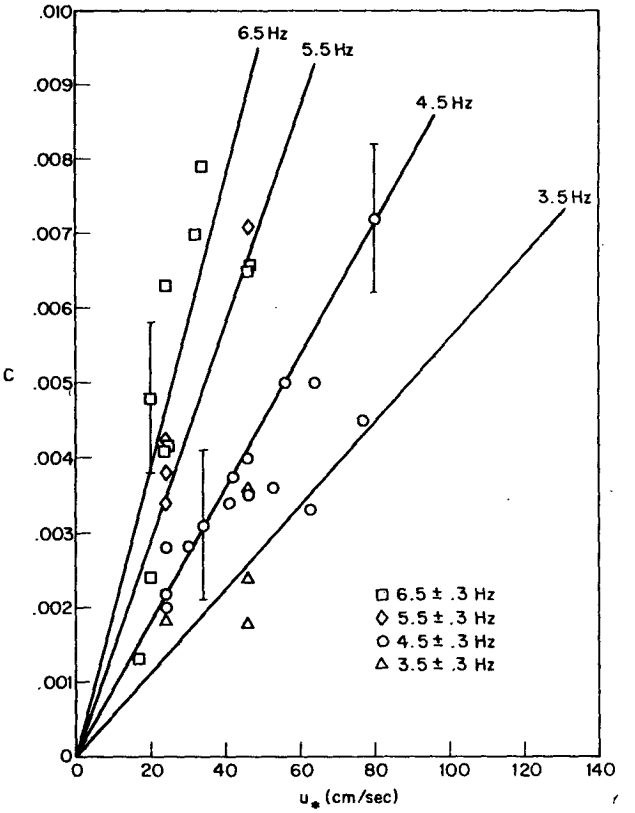

FIG. 10. Equilibrium range "constant" versus friction velocity with dominant wave frequency as a parameter. Lines indicate values used in energy balance calculations.

for the case where $k \ll (g/T)^{1/2}$. Here k_l is given by

$$^3/_2(Tk_l)^{1/2} + U_s = (g/k)^{1/2} + U, \qquad (16)$$

where T is surface tension divided by density, g the acceleration due to gravity, U_s the surface drift, and U the logarithmic, wind-induced drift velocity at a depth of $0.277/k$ below the surface. The non-dimensional equilibrium range "constant" C in Eq. (15) comes from the assumed form

$$E(f) = \frac{C \cos^2\theta}{[k(f)]^4} \qquad (17)$$

for capillary waves.

Surface drift values used in this study were taken from Plant and Wright (1980); they were derived from both phase speed measurements and measurements of transit times of floats. The form of Eq. (17) was checked using Stillwell's photographic technique. Although details of the spectra could not be fit by Eq. (17), mean values of C as a function of f_m and u_* could be obtained by fitting the spectra to k^{-4} curves. The results are shown in Fig. 10 where the lines are empirical fits to the data for various f_m values. These lines were used to obtain values of C for use in Eq. (15).

Fig. 11 gives $S_{nl}^{gg}(f)$ and $S_{nl}^{gc}(f)$ according to these computations for three different peak frequencies and $u_* = 15$ cm s^{-1}. Uncertainty in these curves derives from the experimental spectral densi-

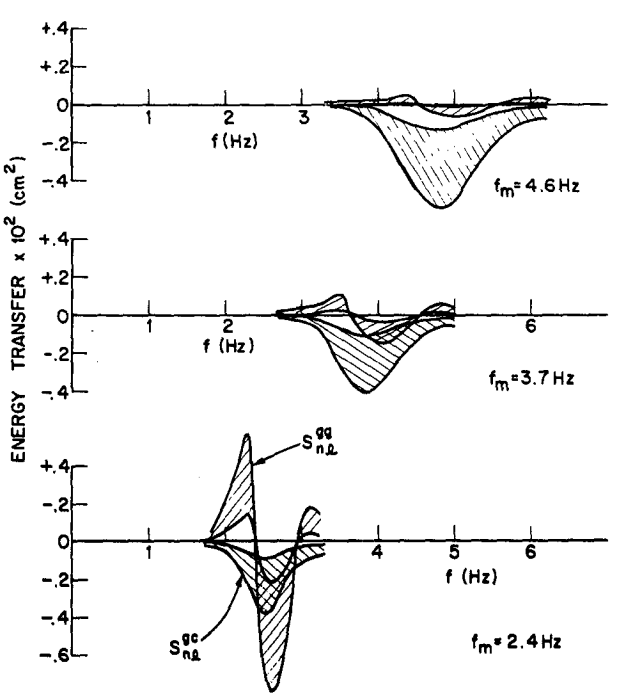

FIG. 11. Energy transfer from gravity (S_{nl}^{gg}) and gravity-capillary (S_{nl}^{gc}) wave theories versus frequency for three dominant wave frequencies and $u_* = 15$ cm s^{-1}.

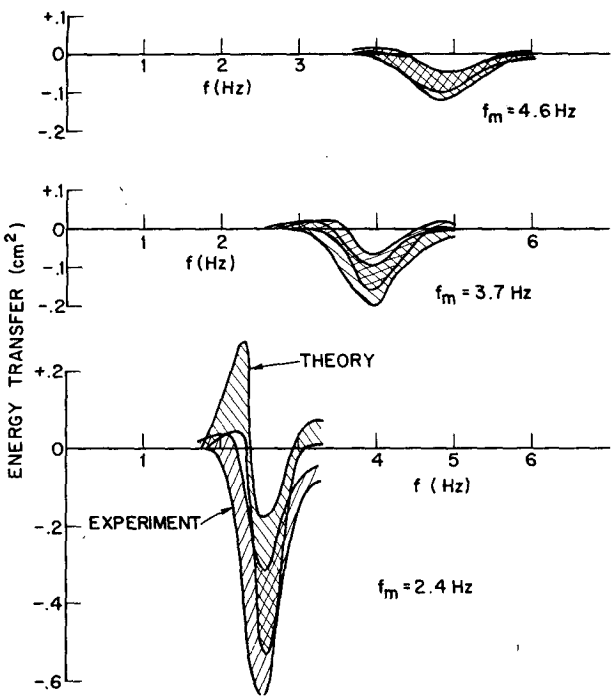

FIG. 12. Experimental and theoretical energy transfer versus frequency for $u_* = 15$ cm s^{-1}. Experimental curve gives $c_g \partial E/\partial x - \beta E$; theory is sum of gravity and gravity-capillary wave theory.

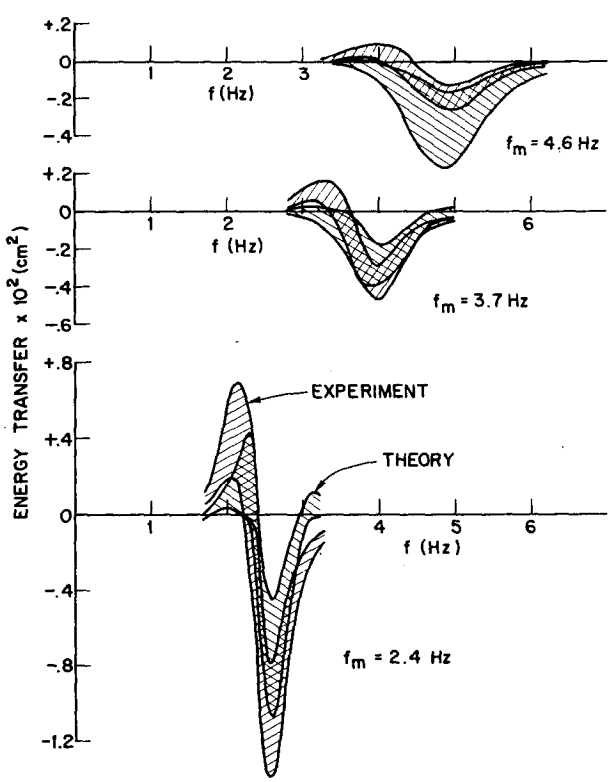

FIG. 13. Experimental and theoretical energy transfer versus frequency for $u_* = 60$ cm s^{-1}.

ties used in the theories. The figure shows that S_{nl}^{gg} dominates for low f_m's while S_{nl}^{gc} dominates for high f_m's; the two interactions are nearly equal for $f_m = 3.5$ Hz in agreement with the conclusions of Valenzuela and Wright (1979). These results varied only slightly for higher wind speeds.

We may now compare the net theoretical energy transfer given by $S_{nl}^{gg} + S_{nl}^{gc}$ with the experimentally determined transfer given by $c_g(\partial E/\partial x) - \beta E$. Figs. 12–14 show these energy fluxes for various peak frequencies and wind speeds. Data for $u_* \leq 60$ cm s^{-1} are consistent with the hypothesis that dissipation plays a minor role in the central part of the spectrum. Nonlinear interactions very efficiently transfer energy to higher frequencies for viscous dissipation or dissipation by wave breaking. The trend of the data, however, indicates that dissipation may become more important at higher wind speeds where experimental energy fluxes are generally of larger magnitude than can be explained by nonlinear interactions. Of course, this could also indicate the need for further consideration of nonlinear effects at high wind speeds.

4. Mechanically generated waves

Waves which exhibited nonlinear effects were easily generated in our tank without airflow using the loudspeaker system and procedures described in Section 2. Fig. 15 shows spectra of the largest waves that we could produce without airflow. These

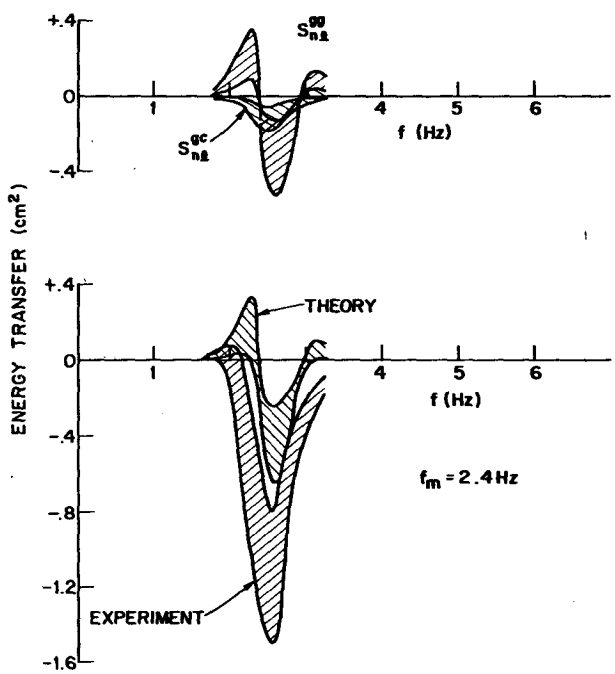

FIG. 14. Energy transfers for $u_* = 100$ cm s^{-1}. Upper curves show gravity (S_{nl}^{gg}) gravity-capillary (S_{nl}^{gc}) wave theories. Lower curves are experimental and theoretical transfers.

spectra were determined using Cox's method at various distances from the wave generator. Variation of this distance was accomplished by rolling the cart, on which the speakers were mounted, toward or away from the fixed slope probe. The duct width was kept constant at 1.25 cm during these runs. While these frequency spectra have a shape similar to wind-wave spectra and exhibit the characteristic shift of the peak toward lower frequencies as fetch increases, they are appreciably smaller and have less angular spread than wind waves. The angular dependence of these waves was once again determined using microwave backscatter and is shown in Fig. 16 for a 15.3 cm wave. In this case, angular wave spectra are sufficiently narrow that convolution with the antenna pattern may somewhat broaden measured spectra at shorter fetches; the antenna pattern is indicated in the figure for comparison. As with wind waves, spectra of mechanically generated waves seem to broaden with increasing fetch, i.e., decreasing dominant frequency. For these narrow spectra, the integral in Eq. (1) was taken to be unity when converting from slope to displacement spectra.

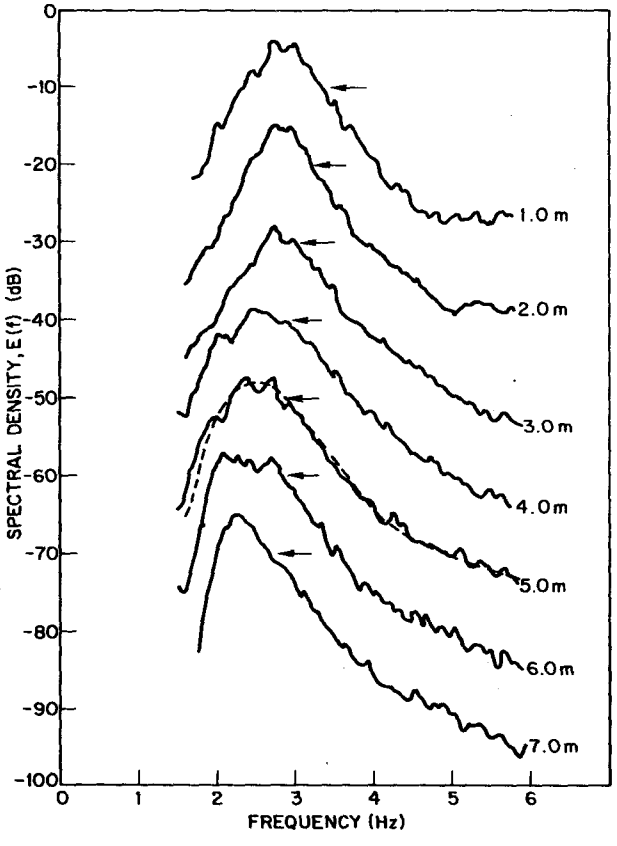

FIG. 15. Spectra of wave systems generated without airflow. Observations were made at the indicated distances from the speaker system. Arrows indicate spectral densities of 0.08 $cm^2\ Hz^{-1}$.

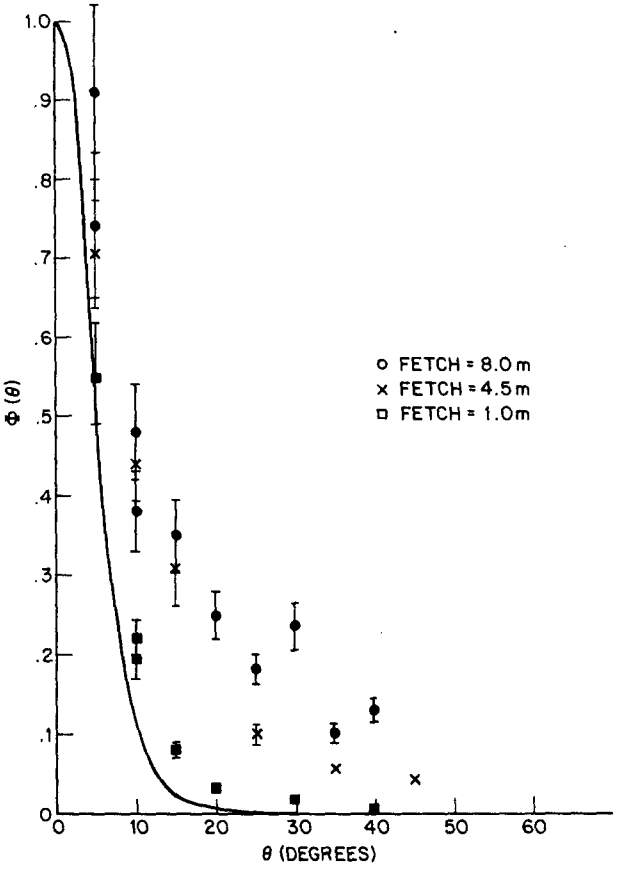

FIG. 16. Angular dependence of 15.3 cm waves generated by the loudspeaker system. Output of the speakers was constant; dominant wave frequency decreased with fetch. The solid line indicates the angular dependence of the antenna pattern.

Comparison of Figs. 3 and 15, show that these mechanically generated waves have significantly smaller peak spectral values than wind waves, by a factor of about 0.14 for $f_m = 2.5$ Hz. Part of this difference is simply due to the different spectral widths. For instance at 5.0 m fetch,

$$0.14 = \frac{\int E_m(f,\theta)d\theta}{\int E_w(f,\theta)d\theta} = \frac{E_m(f,0)\int \Phi_m(\theta)d\theta}{E_w(f,0)\int \Phi_w(\theta)d\theta} \approx \frac{0.43E_m(f,0)}{E_w(f,0)}, \quad (18)$$

where subscripts m and w refer to mechanically generated and wind waves, respectively, and the last step utilizes values of $\Phi(\theta)$ interpolated from Figs. 2 and 16. Thus spectral densities of mechanically generated waves along the tank axis, $E_m(f,0)$, are about one-third of those for wind waves at this fetch and peak frequency, $E_w(f,0)$.

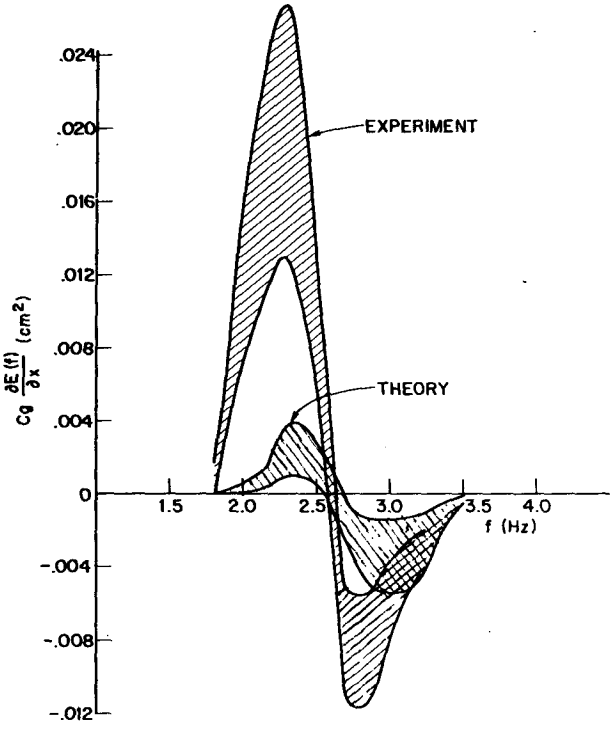

FIG. 17. Experimental and theoretical energy transfers for mechanically-generated wave systems. Experimental curves are $c_g \partial E/\partial x$; theoretical curves show gravity wave theory. Dominant wave frequency is 2.5 Hz.

Other features of the spectra of Fig. 15 are of some interest. Peak spectral values $E(f_m)$ tend to decrease rapidly near the generation point, then increase again farther down the tank. The initial sharp decline of $E(f_m)$ with fetch was observed only when the speaker system was driven near its maximum power levels. The inference is that anomalously large dissipation occurs near the generation area when the generated wave height exceeds a critical level. A shift of the spectral peak to lower frequencies was observed at wave amplitudes well below this critical level. In fact, at fetches > 2–3 m, spectral densities began to saturate well before the speaker system was driven to its maximum power output. Thus measurements of energy transfer reported below were made at fetches longer than 2 m.

The measured net energy transfer, $c_g \partial E(f)/\partial x$, is shown in Fig. 17 for waves generated mechanically at 5.0 m fetch with $f_m = 2.5$ Hz. No scaling of these spectra was attempted; $\partial E(f)/\partial x$ was obtained from curves of $E(f)$ versus fetch. The dispersion relation near the dominant wave frequency was measured using the microwave techniques reported earlier for wind waves (Plant and Wright, 1979). Data conformed exactly to the usual small-amplitude dispersion relation $\omega^2 = gk$ so the group velocity was simply $g/4\pi f$. The figure also shows energy fluxes determined from the gravity-wave theory. The spectral form for these calculations was Eq. (3) with the following parameters:

$$\left.\begin{aligned} \alpha &= 0.0039 \\ \gamma &= 18.0 \\ \sigma &= \begin{cases} 0.50, & f < f_m \\ 0.29, & f > f_m \end{cases} \end{aligned}\right\}. \tag{19}$$

The dashed line in Fig. 15 shows this form. An angular dependence given by $\psi(\theta) = \exp(-|\theta|/\theta_0)/2\theta_0$ with θ_0 chosen to reproduce the data of Fig. 16 was used. No gravity-capillary interaction was computed for these waves since capillary wave amplitudes are very small except near crests, thus implying negligible transfers due to this theory.

Several other measurements of $c_g \partial E/\partial x$ at different fetches and peak frequencies using both slope and capacitance probes have been made. Fig. 18 shows the net source function at 2.1 Hz ($f_m = 2.5$ Hz) as a function of mean-square wave height. Spectra of constant peak frequency but variable amplitude were generated using the speaker system simply by varying the gain of the tape recorder and observing at slightly different fetches. Closed circles are capacitance probe measurements while open circles show measurements obtained from the slope probe; the highest open circle cor-

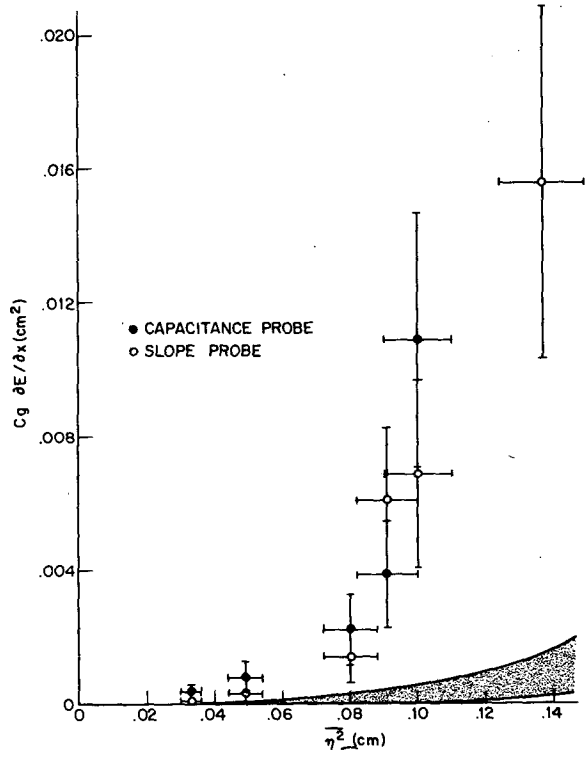

FIG. 18. Net energy transfer at 2.1 Hz versus mean-square height. Dominant wave frequency was 2.5 Hz. Shaded area shows gravity wave theoretical predictions.

responds to the spectra shown in Fig. 15. Energy fluxes predicted by the gravity wave theory for a constant spectral shape are given by the shaded area at the bottom of the figure.

These results, like those shown in Fig. 14, indicate that the observed energy flux is larger than predicted. Errors in the measurements of angular spectra should not affect this conclusion since theoretical energy transfers maximize for spectral widths near those shown in Fig. 16; Hasselmann (1962) has pointed out that energy fluxes for unidirectional spectra vanish to third order, a conclusion also yielded by Longuet-Higgins' (1976) theory.

Furthermore, the theoretical predictions depend on $E(f,0)$ to the third power while the experimental values are obtained from finite-difference evaluation of $\partial E(f)/\partial x$, which would change linearly if $E(f,0)$ were changed. Thus an increase in $E(f,0)$ of a factor of about 3 would be necessary to match theory and experiment for most frequencies. This is well outside estimated experimental uncertainties and, interestingly, is about the same as the ratio of wind wave to mechanically generated wave spectral densities along the tank axis for these conditions. Thus the relationship of spectra to theoretical energy fluxes is consistent with results for wind waves.

5. Discussion and conclusions

When theoretical results depend on the second and third powers of statistical quantities, tests of these theories are necessarily somewhat equivocal on account of the compounding of uncertainties. Nevertheless, some firm conclusions seem warranted by these experiments. The wind wave results indicate that perturbation theory, if both gravity and surface tension are included, predicts energy fluxes in good agreement with those observed in the neighborhood of the dominant wave of short gravity wave systems for $u_* < 60$ cm s^{-1}. Not only is the characteristic shift of the spectral peak to lower frequencies with fetch or wind speed well predicted by these interactions but energy is very effectively transferred to high frequencies for dissipation, even for systems having dominant wave frequencies near 5 Hz. The possibility that dissipation also occurs near the spectral peak is not ruled out by these results but, at moderate wind speeds, its role appears to be subordinate to that of nonlinear interactions as Wu *et al.* (1977) found for the case of wave breaking. At higher wind speeds agreement between experiment and theory degrades somewhat, possibly indicating increased dissipation or other nonlinear transfer.

Energy fluxes in short gravity wave systems which are generated without airflow are not well explained by existing perturbation theory. The theory yields energy transfer which is an order of magnitude too small in some cases. One possible explanation of this could be that first-order spectral components are not completely uncorrelated, an assumption imposed by current theory. If some correlation did exist, transfers of energy could occur, for example, in gravity wave systems at fourth order in the energy expansion instead of sixth (Hasselmann, 1962) and thus would be larger than presently predicted. This effect could also be present in wind-wave systems, especially at high wind speeds, although the data indicate that the correlation would be much smaller.

Taken together with our previous work (Plant and Wright, 1979), these results demonstrate that for many wind speeds and fetches wind-wave systems behave as systems of weakly interacting sinusoidal waves whose energy balance may be described by perturbation theory. This contradicts recent proposals that such theories are inadequate to model wind waves and that these waves behave like nonlinear wavetrains in which all Fourier components travel with a single phase velocity (Lake and Yuen, 1978; Rikiishi, 1978; Toba, 1979). In fact, wave systems generated without airflow in this study obeyed the dispersion relation obtained from linear theory in the neighborhood of the spectral peak. Thus, even though their energy balance is not well modeled by current theory, it is probable that they behave as weakly interacting waves.

It is interesting to relate the results of this study to the work of Alber (1978) on the stability of two-dimensional random surface wavetrains. According to Alber, such wavetrains will be stable under long-wave perturbation if

$$\frac{\sigma_w}{f_m} \geq \sqrt{\overline{S_D{}^2}}, \tag{20}$$

where σ_w is the half-width of the spectral peak at half the maximum intensity. Applying this criterion to the short gravity waves of this investigation, we find that wind waves would be unstable if $u_* > 20$ cm s^{-1}, while the mechanically generated waves always would be stable. According to this, such "Benjamin-Fier" type instabilities should not play a role in the development of the mechanically generated waves.

Finally, our results indicate that the maximum negative value of $S_{nl} + S_d$ does not occur at the frequency of the spectral peak. For both wind waves and mechanically-generated waves, this maximum value always occurs at frequencies higher than f_m. The attractively simple model of gravity-wave nonlinear interactions proposed by Longuet-Higgins (Longuet-Higgins, 1976; Fox, 1976) thus seems to be inadequate to explain our results. Recently, however, Dungey and Hui (1979) have pointed out that Longuet-Higgins theory is only valid for a very narrow spectrum. They introduced a modification

to the theory which accounted for a finite spectral bandwidth to first order in normalized width. Energy transfers calculated to this order attained their maximum negative values at frequencies above that of the dominant wave, in agreement with Hasselmann's work and this study.

Acknowledgments. The author would like to thank Dr. Gaspar R. Valenzuela for the use of his modification of the gravity-gravity wave program and Mr. William C. Keller and Mr. Roger O. Pilon for access to their photographic measurements. The author also gratefully acknowledges many stimulating and rewarding discussions with Dr. John W. Wright.

REFERENCES

Alber, I. E., 1978: The effects of randomness on the stability of two-dimensional surface wavetrains. *Proc. Roy. Soc. London*, **A363**, 525–546.

Barnett, T. P., 1966: On the generation, dissipation, and prediction of ocean wind waves. Ph.D. dissertation, University of California, San Diego, 147 pp.

Cox, C. S., 1958: Measurements of slopes of high-frequency wind waves. *J. Mar. Res.*, **16**, 161–204.

Duncan, J. R., W. C. Keller and J. W. Wright, 1974: Fetch and wind speed dependence of Doppler spectra. *Radio Sci.*, **9**, 809–819.

Dungey, J. C., and W. H. Hui, 1979: Nonlinear energy transfer in a narrow gravity-wave spectrum. *Proc. Roy. Soc. London*, **A368**, 239–265.

Fox, M. J. H., 1976: On the nonlinear transfer of energy in the peak of a gravity-wave spectrum. II. *Proc. Roy. Soc. London*, **A348**, 467–483.

Hasselmann, K., 1962: On the non-linear energy transfer in a gravity-wave spectrum. Part I. General theory. *J. Fluid Mech.*, **12**, 481–500.

——, 1968: Weak-interaction theory of ocean waves. *Basic Developments in Fluid Dynamics*, Vol. 2, Academic Press, 117–182.

——, 1974: On the spectral dissipation of ocean waves due to white capping. *Bound.-Layer Meteor.*, **6**, 107–127.

——, T. P. Barnett, E. Bouws, H. Carlson, D. E. Cartwright, K. Enke, J. A. Ewing, H. Gienapp, D. E. Hasselmann, P. Kruseman, A. Meerburg, P. Müller, D. J. Olbers, K. Richter, W. Sell and H. Walden, 1973: Measurements of wind-wave growth and swell decay during the Joint North Sea Wave Project (JONSWAP). *Dtsch. Hydrogr. Z.*, **A12**, 95 pp.

Hidy, G. M., and E. J. Plate, 1966: Wind action on water standing in a laboratory channel. *J. Fluid Mech.*, **26**, 651–687.

Keller, W. C., and R. O. Pilon, 1980: The directional spectrum of wind-generated waves. In preparation.

Lake, B. M., and H. C. Yuen, 1978: A new model for nonlinear wind waves. Part I. Physical model and experimental evidence. *J. Fluid Mech.*, **88**, 33–62.

Larson, T. R., and J. W. Wright, 1975: Wind-generated gravity-capillary waves: Laboratory measurements of temporal growth rates using microwave backscatter. *J. Fluid Mech.*, **70**, 417–436.

Longuet-Higgins, M. S., 1976: On the nonlinear transfer of energy in the peak of a gravity-wave spectrum: A simplified model. *Proc. Roy. Soc. London*, **A347**, 311–328.

Mitsuyasu, H., 1968: On the growth of the spectrum of wind-generated waves (I). *Rep. Res. Inst. Appl. Mech. Kyushu Univ.*, **16**, 459–482.

——, and T. Honda, 1975: The high-frequency spectrum of wind-generated waves. *Rep. Res. Inst. Appl. Mech. Kyushu Univ.*, **22**, 327–355.

Plant, W. J., 1978: The gravity-capillary wave interaction applied to wind-generated, short gravity waves. NRL Rep. 8289, Naval Research Laboratory.

——, and J. W. Wright, 1977: Growth and equilibrium of short gravity waves in a wind-wave tank. *J. Fluid Mech.*, **82**, 767–793.

——, and ——, 1979: Spectral decomposition of short gravity wave systems. *J. Phys. Oceanogr.*, **9**, 621–624.

——, and ——, 1980: Phase speeds of upwind and downwind traveling short gravity waves. *J. Geophys. Res.*, **85**, 3304–3310.

Rikiishi, K., 1978: A new method for measuring the directional wave spectrum. Part II: Measurement of the directional spectrum and phase velocity of laboratory wind waves. *J. Phys. Oceanogr.*, **8**, 518–529.

Stillwell, D., Jr., 1974: Directional spectra of surface waves from photographs. *J. Geophys. Res.*, **79**, 1277–1284.

Toba, Y., 1974: Macroscopic principles on the growth of wind waves. *Sci. Rep. Tohoku Univ.*, Ser. 5, *Geophys.*, **22**, No. 2, 61–73.

——, 1979: Study on wind waves as a strongly nonlinear phenomenon. *Proc. Twelfth Symp. Naval Hydrodynamics*, Nat. Acad. Sci., 529–540.

Valenzuela, G. R., and M. B. Laing, 1972: Nonlinear energy transfer in gravity-capillary wave spectra, with applications. *J. Fluid Mech.*, **54**, 507–520.

——, and J. W. Wright, 1979: Modulation of short gravity waves by longer-scale periodic flows—a higher-order theory. *Radio Sci.*, **14**, 1099–1110.

Wu, H. Y., E. Y. Hsu and R. L. Street, 1977: The energy transfer due to air-input, non-linear wave-wave interaction and white-cap dissipation associated with wind-generated waves. Tech. Rep. No. 207, Dept. Civil Eng., Stanford University, 158 pp.

——, —— and ——, 1979: Experimental study of nonlinear wave-wave interaction and white-cap dissipation of wind-generated waves. *Dyn. Atmos. Ocean*, **3**, 55–78.